Biophysical Journal
Article

Biophysical Society

Membrane Curvature Revisited—the Archetype of Rhodopsin Studied by Time-Resolved Electronic Spectroscopy

Steven D. E. Fried,[1] James W. Lewis,[2] Istvan Szundi,[2] Karina Martinez-Mayorga,[1] Mohana Mahalingam,[3] Reiner Vogel,[3] David S. Kliger,[2] and Michael F. Brown[1,4,*]

[1]Department of Chemistry and Biochemistry, University of Arizona, Tucson, Arizona; [2]Department of Chemistry and Biochemistry, University of California, Santa Cruz, Santa Cruz, California; [3]Biophysics Section, Institute of Molecular Medicine and Cell Research, Albert-Ludwigs-University, Freiburg, Germany; and [4]Department of Physics, University of Arizona, Tucson, Arizona

ABSTRACT G-protein-coupled receptors (GPCRs) comprise the largest and most pharmacologically targeted membrane protein family. Here, we used the visual receptor rhodopsin as an archetype for understanding membrane lipid influences on conformational changes involved in GPCR activation. Visual rhodopsin was recombined with lipids varying in their degree of acyl chain unsaturation and polar headgroup size using 1-palmitoyl-2-oleoyl-*sn*-glycero- and 1,2-dioleoyl-*sn*-glycerophospholipids with phosphocholine (PC) or phosphoethanolamine (PE) substituents. The receptor activation profile after light excitation was measured using time-resolved ultraviolet-visible spectroscopy. We discovered that more saturated POPC lipids back shifted the equilibrium to the inactive state, whereas the small-headgroup, highly unsaturated DOPE lipids favored the active state. Increasing unsaturation and decreasing headgroup size have similar effects that combine to yield control of rhodopsin activation, and necessitate factors beyond proteolipid solvation energy and bilayer surface electrostatics. Hence, we consider a balance of curvature free energy with hydrophobic matching and demonstrate how our data support a flexible surface model (FSM) for the coupling between proteins and lipids. The FSM is based on the Helfrich formulation of membrane bending energy as we previously first applied to lipid-protein interactions. Membrane elasticity and curvature strain are induced by lateral pressure imbalances between the constituent lipids and drive key physiological processes at the membrane level. Spontaneous negative monolayer curvature toward water is mediated by unsaturated, small-headgroup lipids and couples directly to GPCR activation upon light absorption by rhodopsin. For the first time to our knowledge, we demonstrate this modulation in both the equilibrium and pre-equilibrium evolving states using a time-resolved approach.

SIGNIFICANCE Lipid composition plays a key regulatory role in membrane biochemistry including viral budding, fusion, and signaling by G-protein-coupled receptors (GPCRs). Previous descriptions of membrane lipid-protein interactions cannot explain strong in- and out-of-plane coupling governed by lipid structure. The flexible surface model (FSM) alters this paradigm via formulation of the membrane as a mechanical stress field. We show empirically that membrane curvature stress tightly modulates a significant biochemical process, i.e., signaling by the canonical GPCR rhodopsin. Pump-probe spectroscopy affords high-time-resolution insights confirming strengths of the FSM over previous models.

INTRODUCTION

The concept of nonspecific, mechanical interactions driving physiological processes at the membrane level has gained increasing traction in the biochemical literature (1–8). The critical finding to pave the way for these theories has been the initial observation that membrane lipid composition is governed by precise biological regulation and is frequently a unique, defining feature of diverse tissue and organelle types. Given the crucial role of the biomembrane in signal transduction (9), ion transport (10), viral budding (11), and membrane fusion or fission, this observation gives rise to key questions about the functions of lipids within the membrane—do lipids primarily act as an inert scaffold to more significant proteins embedded in the bilayer, or do

Submitted September 14, 2020, and accepted for publication November 10, 2020.

*Correspondence: mfbrown@arizona.edu

Karina Martinez-Mayorga's present address is Instituto de Química, Universidad Nacional Autónoma de México, Mexico City, Mexico.

Editor: Tommy Nylander.

https://doi.org/10.1016/j.bpj.2020.11.007

they play an active role in membrane biochemistry? One possibility is a signaling function as detailed for prostaglandins and other lipids that act as secondary messengers within the cell (12,13). Still, the high abundance of some lipids, such as those with unsaturated groups within retinal rod disk membranes (RDMs), is unnecessary for purely signaling purposes. The alternate viewpoint is that lipids play a biophysical role in membrane function, an idea that has gained prominence with the concept of rafts (14,15) and functional membrane "patchiness" (16). Although cholesterol typically is implicated in the chemistry of lipid rafts, it is strikingly reduced or absent in RDMs and microbial membranes, which also have tightly regulated lipid compositions (17,18). Moreover, the major features of a scientific problem are often captured by simplified continuum models that may be further refined at the local level. Hence, we turn instead to nonspecific mechanisms of lipid-protein coupling (19) related to the material properties of the membrane.

In this work, we compare alternate biophysical models of lipid-protein interactions with time-resolved experimental data describing lipid influences on the activation of the visual receptor rhodopsin. The fluid mosaic model (FMM) has long permeated biochemistry textbooks through its depiction of the membrane as a largely inert, two-dimensional solvent in which "phospholipids and proteins of membranes do not interact strongly" and "appear to be largely independent" (20). Despite the FMM's long-held popularity, its assumption of protein-lipid independence poses significant problems. For instance, the visual receptor rhodopsin holds a preeminent position in the development of the FMM as the first membrane protein for which rotational (21,22) and translational (23,24) diffusion in the membrane was observed. Yet, it also provides a counterexample to the FMM, as its activation depends strikingly on the membrane lipids (4,5,25). The bilayer properties causing these effects have been initially characterized by fluorescence depolarization measurements (26,27), as well as order parameters determined using solid-state ^{2}H NMR spectroscopy (28,29). Various lipid-protein coupling mechanisms have been proposed to describe these membrane effects, including hydrophobic mismatch (30), deformation (4), lipid phase domains (16), and curvature (31). No matter the precise mechanism, clearly the dependence of rhodopsin on its membrane environment is a noteworthy strike against the accuracy of the fluid mosaic model.

Here, we argue that a new biomembrane model is necessary to replace the FMM that has long been a mainstay of biochemistry. We hypothesize that both strong out-of-plane and in-plane couplings are involved in functional lipid-protein interactions (1,5), formulated by a curvature force field (Fig. 1). As an archetypal system, we assess lipid influences on the function of visual rhodopsin, a canonical member of the highly pharmacologically targeted G-protein-coupled receptors (GPCRs) (33,34). Using time-resolved ultraviolet

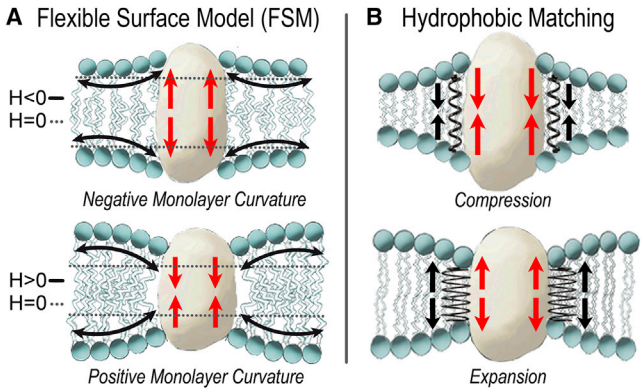

FIGURE 1 Flexible surface model (FSM) and hydrophobic matching descriptions of lipid-protein interactions consider out-of-plane and in-plane deformations of the bilayer. (*A*) In the FSM (1), protein expansion or compression is coupled to deformation of the bilayer curvature, formulated as bending of a neutral plane where the area per lipid is constant. Changes in Gaussian curvature may also occur. Individual lipid pressure profiles cause specific membrane geometries to be energetically favored or disfavored yielding curvature mismatch (frustration). (*B*) In the mattress model (MM), the membrane deformation free energy (32) increases with hydrophobic mismatch between the protein and lipids, driving bilayer expansion or compression at the proteolipid boundary. To see this figure in color, go online.

(UV)-visible spectroscopy, we observe a strong yet reversible coupling between the membrane-bound receptor and the lipids. Strikingly, our discoveries indicate that both acyl chain unsaturation and polar headgroup size are interchangeable in determining proteolipid coupling. Our data consistently imply strong lipid-protein interactions and demonstrate the insufficiency of the fluid mosaic model. Instead, our experiments point to a flexible surface model (FSM) for the coupling between deformation of a continuous membrane surface (5,31) and protein function (Fig. 1 *A*). The FSM is based on the Helfrich formulation of membrane bending energy (35) as we applied for the first time, to our knowledge, to lipid-protein interactions (1,25). Through its introduction of membrane curvature strain, the FSM differs from previously considered hydrophobic matching (32) between Hookean lipid molecules and the protein hydrophobic domains (Fig. 1 *B*). The concept of biomembrane curvature energy applied to protein coupling (1,5) is exemplified here by evidence from time-resolved electronic spectroscopy. Viewing future challenges on the horizon in biochemistry, the FSM framework should enable innovations in pharmaceutical sciences and bioengineering with regard to membrane-bound receptors, channels, virus budding, and fusion.

MATERIALS AND METHODS

Time-resolved and steady-state electronic spectroscopy

All time-resolved spectroscopic measurements were recorded at 30°C after laser photolysis with a 7-ns (80 μJ/mm^{2}), 477-nm light pulse from a

Quanta Ray DCR-2 Nd-YAG pumped dye laser. Bovine rod disk membranes were isolated (Fig. S1), and rhodopsin was exchanged into recombinant membranes as described (36), which were suspended in a low-salt buffer of 10 mM 2-(*N*-morpholino)ethanesulfonic acid (MES) or 1,3-bis(tris(hydroxymethyl)methylamino)propane (BTP) with 30 mM NaCl at pH 5.5, pH 6.5, and pH 8. Each recombinant system entailed a lipid/protein ratio of 100:1. The sample aliquot size was 1 μL in each experimental trial, and the total rhodopsin concentration in each sample was 0.5 mg/mL. At time intervals of 10 μs–50 ms after the pump laser pulse, a 5-μs-duration white light pulse was emitted from a Perkin-Elmer FXQ-856 flashlamp (Waltham, MA). This probe beam was polarized at the magic angle (54.7°) relative to the excitation laser polarization before sample illumination to avoid kinetic artifacts due to rotational diffusion. Optical path lengths were 2 mm for the white light from the flashlamp and 0.5 mm for the laser light. After passing through the sample, the probe light was dispersed and detected using an Andor DH520 intensified CCD detector (Belfast, Northern Ireland, UK) (Fig. S2). Exposed photographic film was used to balance the intensities in different regions of the spectrum so that roughly equal numbers of photoelectrons were produced at all wavelengths during the ~500 ns gate period. Besides time-resolved electronic spectroscopy of recombinant rhodopsin membranes, we conducted steady-state UV-visible measurements of the metarhodopsin equilibrium (Fig. S3). Sandwich samples were prepared with 0.5 nmol of rhodopsin at ~0.8 mg/mL in 200 mM MES or BTP buffers in overlapping pH ranges. These electronic spectra were collected by a Hewlett-Packard 8453 diode array spectrometer (Palo Alto, CA) using a neutral density filter with 10% transmission. Spectra were collected for both the dark-state sample and a metarhodopsin mixture induced by excitation from an array of 520-nm LEDs operating at 16 cd and 20 mA current. Measurements were recorded over a broad range between pH 5 and pH 9.2.

Reduction and analysis of electronic spectral data

Electronic spectra were quantitatively analyzed for metarhodopsin I (MI) and metarhodopsin II (MII) fractions by fitting a linear combination of MI and MII basis spectra to the experimental spectrum, giving the fraction of MII denoted as θ. To account for light scattering changes after bleaching, the experimental difference spectrum was subjected to an inverse-square wavelength scattering correction using the following equation (37): $\Delta A_{corr} = \Delta A - C/\lambda^2 + k$. Here, ΔA_{corr} is the corrected amplitude of the difference spectrum, ΔA is the experimental difference amplitude, C is the fitting constant, λ is the wavelength, and k is an additive constant to correct for baseline shifts. Values of C and k were determined to make the average absorbance change ΔA near 300 nm equal to the average absorbance change near 610 nm. After the scattering correction, a basis spectral fitting method was utilized to determine the relative fractions of the MI and MII states. Experimental basis spectra were collected by varying pH and temperature conditions to completely favor either the MI or MII state for 10 μM rhodopsin in RDMs (see Supporting Materials and Methods). As an additional confirmation, singular value decomposition was performed on a number of difference spectra collected at varying pH conditions to mathematically extract the MI and MII basis components (see Supporting Materials and Methods). The MI-favoring conditions were pH 9.2 and 5°C, whereas the MII-favoring conditions were pH 5.0 and 15°C (Fig. S3). A linear combination of these basis spectra was fitted by the method of least squares to the experimental difference spectrum: $\Delta A(\lambda) = c_1 \Delta A_{MI}(\lambda) + c_2 \Delta A_{MII}(\lambda)$. The positive coefficients c_1 and c_2 reflect the relative contributions of either MI or MII to the total photoactivated rhodopsin system. The total MII fraction θ was therefore calculated as $\theta = c_2/(c_1 + c_2)$, which was plotted as a function of both bulk solution pH and the local membrane surface pH (Figs. S4 and S5). The random spectral errors were estimated as ± 4% with this method. For time-resolved experiments, these uncertainties were propagated with variations from pH fluctuations due to the low-salt buffer conditions to obtain the ± 4–6% error bars shown in the data figures.

RESULTS

To determine the role of membrane composition in rhodopsin activation, we monitored the (inactive) metarhodopsin I–(active) metarhodopsin II equilibrium (38) using time-resolved UV-visible spectroscopy (Figs. S1 and S2). This pump-probe method has been experimentally applied to elucidating critical aspects of the photoactivation mechanism (39–43) in terms of kinetics and thermodynamics. The use of time-resolved UV-visible spectroscopy affords extraordinary control in observing this metastable equilibrium, because of instability at high temperatures that induces rapid conversion to metarhodopsin III (44) or opsin over a timescale of seconds. Moreover, on the fast timescale that the measurements are made, the progress of the reaction from the earlier photointermediates to the development of an equilibrium fraction of metarhodopsin II can be determined.

Photoactivation of rhodopsin is affected by nonlamellar-forming lipids

Spectral changes of rhodopsin in recombinant lipid membranes after λ = 477-nm actinic photoexcitation were measured using a multichannel detector in time increments spanning 10 μs–50 ms (Fig. 2). Time-resolved spectroscopic measurements were made for rhodopsin in a variety of lipid systems, including 1-palmitoyl-2-oleoyl-*sn*-glycero-3-phosphocholine (POPC), 1,2-dioleoyl-*sn*-glycero-3-phosphocholine (DOPC) (Fig. 2 *A*), a 3:1 mixture of 1,2-dioleoyl-*sn*-glycero-phosphoethanolamine (DOPE) with DOPC (Fig. 2 *B*), and the native rod disk membranes (Fig. 2 *C*). Lipids were chosen to represent a diversity of acyl chain types (i.e., saturated palmitoyl groups versus unsaturated oleoyl groups), to distinguish between effects of large (i.e., phosphocholine) and small (i.e., phosphoethanolamine) headgroups, and to represent lipid systems with nonlamellar phase transitions in the low-temperature regime (45,46). A 100% DOPE mixture could not be used because of the formation of an inverted cubic phase under standard conditions (47). Our measurements enabled the construction of pH titration curves describing rhodopsin activation in each recombinant lipid membrane studied.

By carrying out the spectroscopic measurements at three different pH values for each system, we measured how the pH-dependent titration curves for rhodopsin activation shift in the variable presence of RDM, POPC, DOPC, or DOPE lipids (Fig. 3). Rhodopsin (Rh) activation depends on a proton uptake by Glu^{134} of the E(D)RY motif according to the reaction mechanism $Rh + h\nu \rightarrow MI \rightleftharpoons MII_a \rightleftharpoons MII_b + H_3O^+ \rightleftharpoons MII_bH^+$, in which the MII substates are denoted by MII_a and MII_b (40,48,49). The fraction of metarhodopsin II (θ) as a function of pH was determined by fitting the experimental light minus the dark difference spectra with basis (reference) spectra of the MI and MII forms (Fig. S1). A phenomenological Henderson-Hasselbalch pH titration

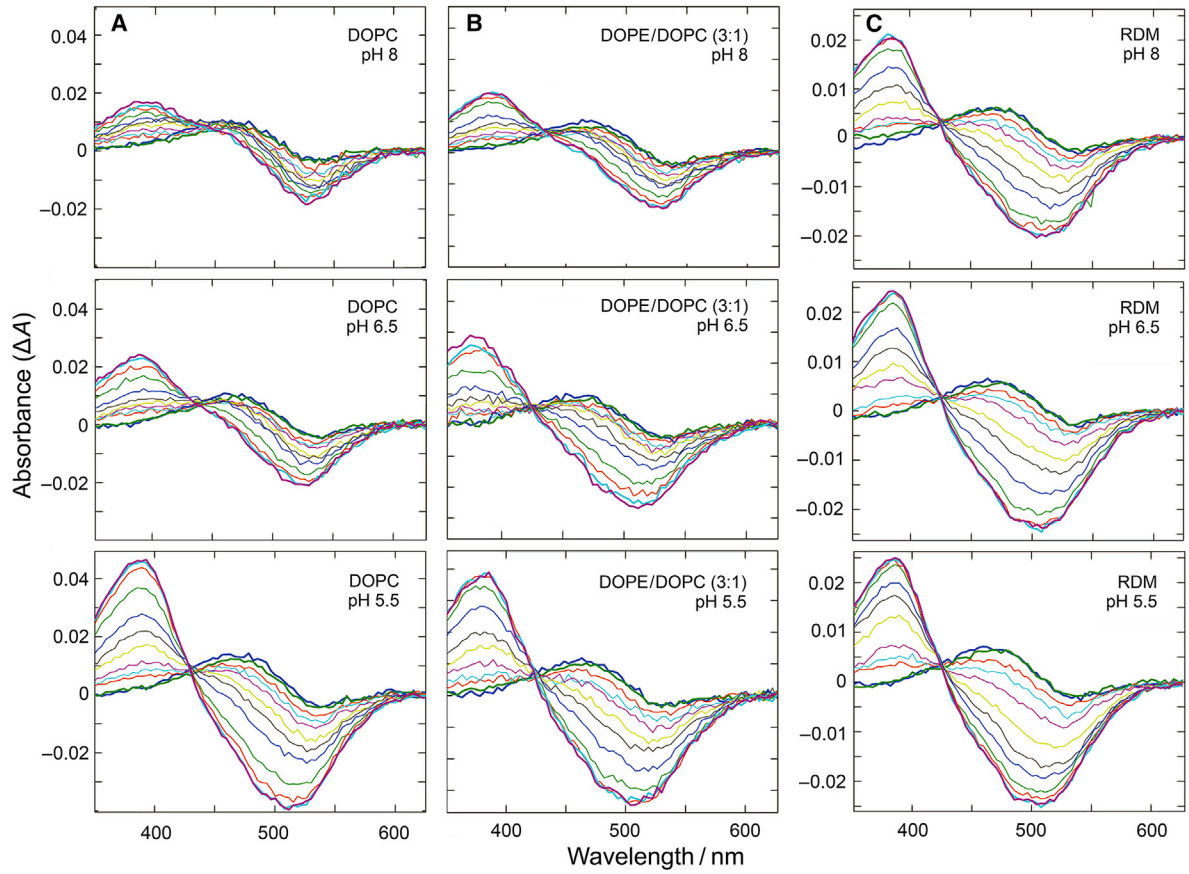

FIGURE 2 Time-resolved UV-visible spectroscopy reveals influences of neutral lipid substitutions on the light-activated metarhodopsin II (MII) state. Difference spectra (*light minus dark*) monitor rhodopsin activation at various pH values in (*A*) DOPC, (*B*) DOPE/DOPC (3:1), and (*C*) native RDM lipid environments (30°C). The recombinant lipid/protein ratio was 100:1. Samples contained 10 mM MES or BTP buffer with 30 mM NaCl. The pump-probe delays were 10, 20, 50, 100, 200, 500 μs, 1, 2, 5, 10, 20, 50 ms in ascending order at 380 nm. Note that low pH and increasing phosphatidylethanolamine lipids cause a shift to the MII state (λ_{max} = 380 nm). To see this figure in color, go online.

curve was fitted to the data points (48): $\theta = (\theta_{alk} + 10^{pK_A-pH})/(1 + 10^{pK_A-pH})$. Here, the measured p$K_A$ value corresponds to the protonation of Glu^{134} in the second of two ionic-lock switches that govern rhodopsin activation, and θ_{alk} denotes the MII fraction observed in the alkaline limit of the pH titration curve because of higher-enthalpy substates MII$_a$ and MII$_b$ that persist at greater temperatures independently of the protonation of Glu^{134}.

We observed that the Glu^{134} pK_A was highly regulated by the lipid environment, in agreement with a modulation of the metarhodopsin conformational equilibrium that couples directly to the acid-base chemistry of Glu^{134}. The highest-value pK_A was observed for the native RDMs, indicating lipid conditions that reversibly favor the MII state. This was followed by the 3:1 DOPE/DOPC lipid environment, pure DOPC, and then pure POPC (Fig. 3 *A*). In relation to the lipid structures, the bulky methylated PC headgroups back shift the equilibrium to the inactive MI state relative to the smaller PE headgroups. A separate trend is observed for the lipid unsaturation: highly unsaturated (1,2-dioleoyl) lipids favored the active MII more than saturated palmitoyl acyl chains. This trend continues to the native RDM lipids, known for their abundance of polyunsaturated ω-3 fatty acids such as docosahexaenoic acid (19,25,50). A variety of models have been proposed to describe lipid-protein interactions that we analyze here for their relation to our new experimental data.

How can we formulate lipid-protein interactions in cellular biomembranes?

Our development is strongly grounded in principles of surface chemistry and physics. A number of mechanisms for lipid-protein coupling may exist in a lipid membrane, making the adoption of a unified, self-consistent model challenging. However, we show here that abandoning the molecular view of membranes in favor of a macroscopic, surface depiction is advantageous toward describing the major types of lipid-protein interactions. In the FSM, the membrane is viewed through the lens of differential geometry as an elastic surface capable of bending and stretching according to the Helfrich free-energy model (35). We consider two primary energetic contributions

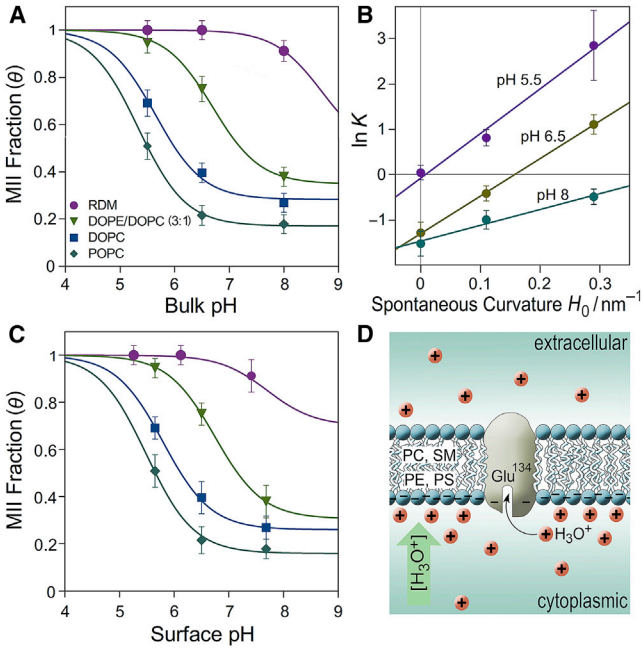

FIGURE 3 Membrane curvature and electrostatics both govern MII formation and may be distinguished from one another. (*A*) Fraction of MII state versus bulk solution pH for various lipid environments at 30°C (lipid/protein ratio of 100:1) is shown. (*B*) Linear dependence of ln *K* on absolute monolayer spontaneous curvature for the MI–MII equilibrium at each pH is consistent with the FSM (1,5). (*C*) Titration curves versus local pH at the membrane surface calculated with the Gouy-Chapman model are shown. (*D*) An illustration of how negatively charged groups of lipids or proteins yield formation of an electrical double-layer of hydronium ions at the membrane surface is given. Uncertainties in the MII fraction (θ) and ln *K* were propagated from estimated errors in the spectral measurements (± 4%) and pH measurements (± 0.1 pH unit). Error bars represent experimental uncertainties of ± 4–6% for the MII fraction. Note that higher local hydronium concentration drives protonation of Glu^{134}, yielding formation of the active MII state. To see this figure in color, go online.

of lipid-protein coupling: the membrane elastic deformation energy, ΔG^{o}_{el}, and solvation energy arising from the proteolipid interfacial tension, ΔG^{o}_{solv} (1,51). The sum of both contributions gives the total lipid-protein coupling energy: $\Delta G^{o}_{LP} = \Delta G^{o}_{el} + \Delta G^{o}_{solv}$. We demonstrate how both of these terms arise logically from the FSM framework and may be quantified by a continuum mechanics approach.

The flexible surface model describes reversible lipid-protein interactions by a curvature elastic force field

In the FSM, the elastic energy of the membrane is attributed exclusively to membrane curvature (bending) (Fig. 1 *A*). Any point on a two-dimensional surface is characterized by two principal curvatures along either axis, expressed as c_1 and c_2, where $c_1 = 1/r_1$ and $c_2 = 1/r_2$ for radii of curvature r_1 and r_2. Both principal curvatures may be combined into a mean curvature H, where $H = (1/2)(c_1 + c_2)$, and a Gaussian curvature $K = c_1c_2$ that is invariant to bending on a simply connected surface free of stretching. Hence, the elastic energy describing curvature deformation of a surface is expressed in terms of both the Gaussian curvature and the displacement of the mean curvature H from the spontaneous curvature H_0 at the energy minimum (35). By modeling the elastic bending energy with a harmonic (Hookean) approximation and making these variable substitutions, the curvature free energy describing the bending of a surface S into a shape described by (r_1, r_2) is given by the integral (5,35)

$$\oiint_S g_c dA = \oiint_S \left[(\kappa/2)(1/r_1 + 1/r_2)^2 + \overline{\kappa}/(r_1 r_2)\right] dA. \quad (1)$$

Here, the free-energy density g_c is related to the mean curvature H through the bending modulus κ and to the Gaussian curvature K by the modulus of Gaussian curvature $\overline{\kappa}$. One can separate the Gaussian curvature term $1/r_1r_2$ to arrive at the following simple expression for the free-energy density at any point (5,35):

$$g_c = \kappa(H - H_0)^2 + \overline{\kappa}K. \quad (2)$$

The natural consequence of this equation is a tendency of the surface to deform to a mean spontaneous curvature H_0 to minimize the free energy. A bilayer exhibiting frustration or nonminimized free energy is capable of performing work on protein-lipid systems through coupling between membrane deformation and protein conformational changes (1).

According to the FSM, the free energy of curvature plays a principal governing role in the modulation of protein chemical equilibria that involve changes in membrane deformation. If one considers a transition from a state with mean curvature H_1 to a state with mean curvature H_2, the free-energy density change of the deformation is calculated as $\Delta g_c = \kappa(H_2 - H_0)^2 - \kappa(H_1 - H_0)^2$. Rearranging this expression then yields $\Delta g_c = -2\kappa(H_2 - H_1)H_0 + \kappa(H_2^2 - H_1^2)$. Taking a first-order approximation and assuming that the curvature of the initial state H_1 is zero (a feature of the metarhodopsin I state), then we determine the following term for the molar elastic free-energy change per protein molecule (1,5):

$$\Delta G^{o}_{el}/N_A = \Delta G^{o}_{c}/N_A = -2\kappa(A_L H_2 N_L)H_0. \quad (3)$$

In this formula, A_L describes the cross-sectional area per lipid, N_A the Avogadro constant, and N_L the number of lipids per protein. We make the simplifying assumption that the value of H_0 is approximately given by the inverse of the water radius of curvature (R_W) of the hexagonal phase (H_{II}) nanotubes of the lipids under conditions of dual solvent stress (52). For a conformational change of a membrane protein, the equilibrium constant is $K = \exp(-\Delta G^{o}/RT)$. It follows that a linear relationship exists between ln *K* and the spontaneous curvature H_0 of a membrane system, with a positive slope given by the

expression $2\kappa(A_L H_2 N_L)N_A/RT$. Indeed, such a relationship is observed experimentally for rhodopsin at each pH tested (Fig. 3 *B*). Varying the membrane spontaneous curvature (53) by altering the recombinant lipid bilayer composition of POPC, DOPC, and DOPE/DOPC (3:1) systematically adjusts the metarhodopsin equilibrium in accordance with the linear model of Eq. 3. Using the above expression for the slope, we may estimate the final monolayer curvature H_2 corresponding to the MII state for each pH value. To make a heuristic calculation, we assume that $A_L = 70$ Å^2, $N_L = 50$ lipids per rhodopsin per monolayer, and $\kappa = 10\ k_BT$ (51). Close to the membrane isoelectric point (p$I = 4.3$ for RDMs and 7.3 for recombinant membranes), we calculate a final radius of curvature of ~700–800 Å. Under more alkaline conditions (pH 8), the monolayer takes on a greater negative charge (54), causing a larger radius of curvature in the final MII state (Fig. 3 *B*).

The proteolipid solvation energy counterbalances the elastic energy of membrane deformation

Additionally, the energy of hydrophobic packing interactions at the lipid-protein interface (1,55) is governed by both the strength of the protein-lipid interactions at the interface (i.e., surface tension γ_{LP}) and the surface area A_P of the protein interacting with the lipids. Given a change in state that alters the protein surface area by $\Delta A_P \equiv A_{P2} - A_{P1}$, the molar free-energy change due to solvation is

$$\Delta G^o_{solv}/N_A = \gamma_{LP}\Delta A_P. \quad (4)$$

Another way of viewing this type of protein-lipid interfacial tension, responsible for sealing the protein into the membrane, is through the concept of a Laplace pressure. A curved interface exists between the protein and membrane lipids, causing a surface tension-induced pressure differential similar to that responsible for capillary action and related phenomena (1). The pressure differential between the protein and lipids will then be given by $\Delta P \equiv P_P - P_L = \gamma_{LP}(1/r_1 + 1/r_2)$, where γ_{LP} describes the proteolipid surface tension and r_1 and r_2 describe the two principal radii of curvature. For the sake of illustration, one can assume a cylindrical transmembrane protein shape, wherein one of the radii of curvature becomes infinite and the Laplace pressure becomes $\Delta P = \gamma_{LP}/r$. Integrating this pressure over the surface area displacement undergone during a protein conformational change gives a surface work term equivalent to a free energy change (1).

Hence, for a change in state of a protein with intramembranous surface area A_{P1} to a state with area A_{P2}, the free-energy contribution due to chain packing is given by Eq. 4. Equivalently, this same term has been expressed through a dependence on hydrophobic mismatch: $\Delta G_{solv} = \sigma_L g_{mis}\Delta|L_L - L_P|$ (55). Here, σ_L describes the lipid width (related to lipid cross-sectional area A_L by $\sigma_L = \sqrt{A_L}$), g_{mis} corresponds to the free-energy density of hydrophobic mismatch, L_L denotes the lipid length, and L_P is half the protein hydrophobic length. As a result, $\Delta|L_L - L_P|$ describes the difference in hydrophobic mismatch between the two states of the protein-membrane system. Note the equivalence to Eq. 4, in which g_{mis} is a descriptor of the surface tension γ_{LP} and in this term $\sigma_L\Delta|L_L - L_P| = \Delta A_P$, assuming longitudinal expansion in the protein and negligible deformation of the lipids themselves.

Combining both membrane curvature and solvation interfacial tension contributions, we thus obtain the following expression for lipid-protein coupling energies (5):

$$\Delta G^o_{LP}/N_A = -2\kappa(A_L H_2 N_L)H_0 + \gamma_{LP}\Delta A_P. \quad (5)$$

By considering membrane surface properties in the flexible surface model, we determine two major energetic contributions to protein-lipid interactions: the curvature elastic energy ΔG^o_{el} described by the bending modulus κ and chain packing (solvation) energy ΔG^o_{solv} described by the surface tension γ_{LP} at the proteolipid interface. A balance exists between these two terms for transitions such as the conversion of MI to MII, which entails a structural expansion of rhodopsin. The first (elastic) term is negative and corresponds to a favorable driving force for the conformational change because the membrane lipids adopt a structure closer to their inherent, spontaneous curvature. The second (solvation) term, on the other hand, is positive because hydrophobic mismatch at the proteolipid interface increases upon MII formation. Consequently, a balance of both elastic and solvation energies modulates rhodopsin activation in the FSM.

In hydrophobic matching, the membrane elastic energy is due to thickness or area deformation

Alternatively, elastic energy may exist in the form of membrane thickness or area deformation (1,25). By maintaining the continuum mechanics view outlined in the FSM, it is possible to take a further step by allowing stretching of the continuous membrane surface, treated with a harmonic approximation described by an area elastic modulus, K_A. For incompressible materials, a correspondence exists between area deformation (25) and thickness deformation (32), which has been described in the literature as hydrophobic mismatch (30,55). Following Gibson and Brown (25), the molar free energy per individual lipid in a monolayer due to elastic area deformation is formulated in an analog of Hooke's law as

$$G_t/N_A = (1/2)K_A(A_L - A_{L0})^2/A_{L0}. \quad (6)$$

The free-energy density is given in terms of the area elastic modulus K_A (56), which is related to the surface tension γ_{LW} at the lipid-water interface (25) by $2\gamma_{LW}$ for a monolayer and $4\gamma_{LW}$ for a bilayer (25,51). In addition, A_L describes the perturbed surface area per lipid and A_{L0} the

nonperturbed area, where it is assumed the deformations to the lipid area are sufficiently small that a harmonic approximation is applicable. By relating this type of membrane deformation to the area per lipid and area elastic modulus, we obtain an expression that is closely tied to experimental observables, namely the lipid order parameters that are measurable by solid-state ^{2}H NMR spectroscopy (56).

An equivalent formulation is the frequently discussed mattress model (MM), based on a thickness elastic strain due to stretching or compressions of individual lipids (Fig. 1 *B*) in response to hydrophobic mismatch (30,32,55,57). Here again, we recognize that lipid bilayer area deformation must be accompanied by a corresponding deformation in thickness. Deformation of a material is generally described by Young's modulus and Poisson's ratio (56). Assuming the lipids are incompressible, then the area and thickness deformation must be inversely proportional, with the relationship between transverse and longitudinal strain given by the Poisson ratio $\nu = 1/2$ (56). Using a harmonic approximation, one may then consider individual lipids as Hookean objects whose longitudinal stretching or compression give a thickness-mediated elastic energy G_t proportional to the square of the lipid displacement (55):

$$G_t/N_A = (1/2)K_tA_{L0}(L - L_0)^2/L_0. \quad (7)$$

In this formula, K_t is the thickness elastic modulus (or Young's modulus) describing longitudinal compression of individual lipids in a monolayer, where L denotes the perturbed lipid length and L_0, the unperturbed length (55). The thickness modulus is related to the area extension modulus K_A by $K_t = 4\nu^2K_A/L_0$, where ν is Poisson's ratio. For an incompressible yet deformable material, $\nu = 1/2$ and $K_t = K_A/L_0$ for a monolayer, or equivalently $K_t = K_A/D_{B0}$ for a bilayer. In the latter case, we make the substitutions of $D_B = 2L$ and $D_{B0} = 2L_0$ for the thickness of two opposed lipids in place of L and L_0, obtaining an isomorphous form of Eq. 7 whose free energy is twice that of the monolayer (55,56).

It follows that for small deformations, a direct correspondence exists between Eqs. 6 and 7 formulated in terms of lipid length (55), bilayer thickness (56), or cross-sectional area (25). In the hydrophobic mismatch or mattress model (32), free energy inherent to either area (25) or thickness (55,56) deformation of a lipid bilayer (Eqs. 6 and 7) is the sole elastic energy term in the coupling to conformational equilibria of the membrane protein. Then, if we consider a change in state from a membrane of lipid length L_1 to L_2, the molar free-energy change per protein is given by

$$\Delta G^o_{el}/N_A = \Delta G^o_t/N_A = K_tN_LA_{L0}\left[(\Delta L^2/2L_0) - \Delta L\right], \quad (8)$$

in which N_L is the number of lipids per protein. Here, we define $\Delta L^2 \equiv L_2^2 - L_1^2$ and $\Delta L \equiv L_2 - L_1$. As in Eq. 7, for a bilayer we substitute D_B and D_{B0} in place of L and L_0, giving a free-energy change whose value for the same N_L is twice that of the corresponding monolayer—as it must, because free energy is extensive. To first order, this free-energy change due to membrane thickness deformation is most nearly given by $\Delta G^o_t = -K_tN_AN_LA_{L0}\Delta L$ in terms of the lipid length and equivalently for the bilayer thickness. By consequence, the hydrophobic matching framework of the mattress model (32) produces an alternate term describing membrane elastic energy based on thickness or area deformation (25,30,55), and is dependent on membrane lipid length. The combination of this elastic term and the solvation contribution ΔG^o_{solv} yields the total free energy of lipid-protein coupling (32,55).

Note that thus far in the hydrophobic matching or MM treatment of lipid stretching, only the free energy of the individual lipids has been considered. In a simplified case, the concept of a persistence length may be introduced to describe the effective range over which lipids deform because of hydrophobic mismatch (57). The introduction of a persistence length brings us back to the concept of a membrane curvature. As individual membrane lipids compress or extend, determined by their proximity to a transmembrane protein, the membrane surface undergoes a continuous deformation that can be described by the language of differential geometry. Rather than introducing this curvature through a persistence length, however, we have proposed an FSM that is directly formulated on the basis of curvature elastic strain, rather than purely thickness elastic strain (1,25,68).

At this juncture, we conclude that there exist at least three possible coupling interactions between the bilayer and integral membrane proteins: curvature, lipid-protein interfacial tension, and thickness or area deformation, which is also related to the lipid-water interfacial tension (1,25). When comparing the various proposed models, we note the FMM assumes independent protein and lipid behavior; it includes none of these terms (20). The MM contains ΔG^o_t and ΔG^o_{solv} terms in accordance with a hydrophobic mismatch and longitudinal tension on the lipids (32). The FSM, by considering membrane curvature as a source of elastic energy, contains the ΔG^o_c and ΔG^o_{solv}terms. Notably, by virtue of its consideration of bending energy (5,31), only the FSM describes both in- and out-of-plane coupling interactions in the membrane (Table 1).

TABLE 1 Free-Energy Terms Considered in each Model of Protein-Lipid Interactions

Model	Contributions to Lipid-Protein Coupling
Fluid mosaic model (FMM)	$\Delta G^o_{LP} = 0$
Hydrophobic matching/Mattress model (MM)	$\Delta G^o_{LP} = \Delta G^o_t + \Delta G^o_{solv}$
Flexible surface model (FSM)	$\Delta G^o_{LP} = \Delta G^o_c + \Delta G^o_{solv}$

Standard Gibbs free-energy changes due to lipid-protein interactions (LP) are designated as follows: membrane thickness deformation (t); lipid solvation of intramembranous protein surface (solv); and lipid monolayer curvature deformation (c) (see text).

Rhodopsin activation depends on the local hydronium ion concentration at the membrane surface

Besides membrane curvature effects on rhodopsin activation, electrostatic properties of the membrane can also modulate rhodopsin conformational dynamics. Membrane electrostatics influence local pH-buffering at the bilayer surface (Fig. 3 *C*) because of titratable groups of rhodopsin and the lipid headgroups, which may recruit hydronium ions to protonate Glu^{134} of the E(D)RY motif (Fig. 3 *D*). Specifically, charged phosphoserine (PS) and zwitterionic phosphoethanolamine (PE) headgroup lipids are predominantly located in the cytoplasmic leaflet of the rod disk membranes, whereas charge-neutral phosphocholine (PC) lipids and sphingomyelin (SM) mainly reside in the extracellular leaflet (54,58). Thus far, we have dealt with apparent pK_A values in terms of the bulk solution pH. Yet, for a surface containing titratable groups, the pH will be locally buffered according to Poisson-Boltzmann statistics, leading to a shifting and broadening of the titration curve in terms of the bulk pH.

As a result, we can calculate a local pH from the surface potential to yield a Henderson-Hasselbalch titration curve in terms of the intrinsic pK_A value. To take into account the electrostatic influences of the protein, lipids, and aqueous buffer on the MI–MII equilibrium (59), we use the Poisson-Boltzmann equation for a planar surface to calculate the surface (local) pH of the membrane. This treatment can be further extended in terms of the electrochemical potential μ_i by including the electrostatic potential ψ, leading to $\overline{\mu}_i \equiv \mu_i + \mu_i^{\mathrm{el}}$, where $\mu_i^{el} = z_i F\psi$ is the electrical energy, z_i is the ion charge, and F is Faraday's constant. Because the electrochemical potential for hydronium atoms must be equal at the membrane surface ($\psi = \psi_0$) as in the bulk solution ($\psi = 0$), the potentials are equated to yield the Nernst equation:

$$\mathrm{pH}_{\mathrm{surface}} = \mathrm{pH}_{\mathrm{bulk}} + zF\psi_0/2.303RT. \tag{9}$$

Even though the electrostatic surface potential of the membrane is not directly measurable in these experiments, it can be related to surface charge density by the Poisson-Boltzmann equation, which for a planar surface gives the Gouy-Chapman result,

$$\sigma = \left(C^{1/2}/A\right)\sinh(zF\psi_0/2RT). \tag{10}$$

Here, σ is the membrane surface charge density, ψ_0 is the membrane surface potential, C is the molarity of cations in the BTP or MES buffer, z is the charge of the respective cations, and $A = 134.8\ \mathrm{M}^{1/2}$, the Gouy-Chapman parameter. Note that in the Gouy-Chapman formula, the electrical potential ψ_0 is not an additive function, whereas the surface charge density σ can be decomposed into $\sigma = \sigma_L + \sigma_P$ for the lipid and protein components. The surface charge density for the lipids is negligible in the case of neutral POPC, POPE, and DOPE lipids. For native rod disk membranes, however, it is significant because of the presence of charged phosphoserine headgroups (54,60), as well as the protein rhodopsin (see Supporting Materials and Methods). Because surface charge density σ is dependent on local pH encountered by titratable groups, a nonlinear system of equations results between the Gouy-Chapman model with directly calculated charge density σ, and the Nernst equation relating the hydronium electrochemical potential at the membrane and in the bulk solution. The two independent variables are the local pH and surface potential ψ_0. Such a system can be iteratively solved (61) for a given bulk pH to yield the local pH at the membrane surface (Figs. S4 and S5).

Membrane lipid influences on rhodopsin photoactivation are observed with time-resolved electronic spectroscopy

Coming back to our experimental findings, a significant impact of the membrane lipid composition on rhodopsin function is seen: increasing either lipid saturation or the proportion of phosphatidylcholine lipids back shifts the equilibrium to the inactive MI state, compared to the native rod disk membranes (Fig. 4). For the first time to our knowledge, the results of time-resolved UV-visible spectroscopy indicate how membrane lipids influence attainment of the metarhodopsin equilibrium (Fig. 4 *A*). In comparison with

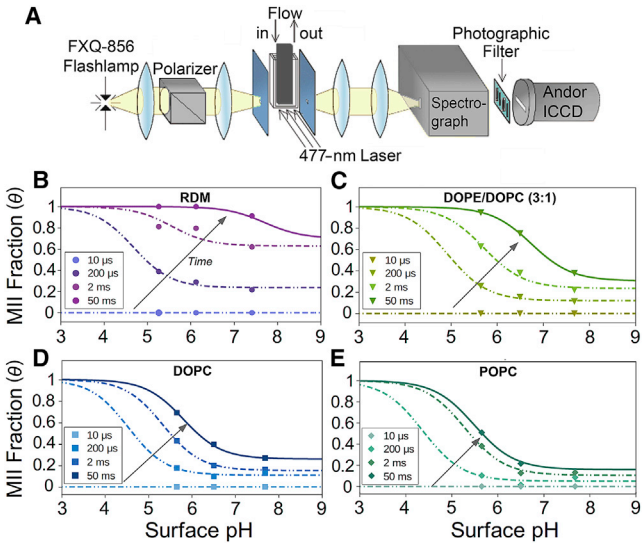

FIGURE 4 Time-resolved electronic (UV-visible) spectra reveal pH- and lipid-dependent attainment of the metarhodopsin equilibrium. (*A*) Schematic of the apparatus used for data collection with microsecond resolution is shown. (*B–E*) Time evolution of the MII state from MI is plotted showing MII fraction (θ) versus local (surface) pH. Rhodopsin activation depends on both pH and time, according to the mechanism $\mathrm{Rh} + h\nu \rightarrow \mathrm{MI} \rightleftharpoons \mathrm{MII_a} \rightleftharpoons \mathrm{MII_b} + \mathrm{H_3O^+} \rightleftharpoons \mathrm{MII_bH^+}$. To guide the eye, Henderson-Hasselbalch curves are plotted through the data. To see this figure in color, go online.

the native RDM lipids (Fig. 4 *B*), the smallest pK_A shift is observed in the case of the small-headgroup, unsaturated DOPE lipids (Fig. 4 *C*), which most resemble the native environment. By substituting these small headgroups with larger, methylated PC groups, the pK_A shift increases in the case of DOPC lipids (Fig. 4 *D*). The largest pK_A shift is observed in the case of POPC membranes, whose phospholipids include one saturated palmitoyl (16:0) and one unsaturated oleoyl (18:1) fatty acid, together with a phosphocholine headgroup (Fig. 4 *E*).

Although some of these differences may be attributed to local variations in hydronium concentration, the same significant trend occurs when these surface pH effects are accounted for with the Gouy-Chapman model (51,61). The negatively charged PS headgroup lipids increase the apparent pK_A of rhodopsin in the rod disk membranes because of an increased local concentration of hydronium ions near the bilayer surface that drives forward the rhodopsin activation to protonated MII (50,54,61,62). Yet this effect can only partially explain the RDM results, and it has no bearing for membranes with zwitterionic headgroups, such as those with POPC, DOPC, and DOPE lipids. Even if the localized variations in hydronium concentration are accounted for, i.e., as when MII fraction is plotted against calculated surface pH rather than against bulk pH, differences in the pK_A of greater than two pH units still persist between rhodopsin in the POPC and RDM systems. Electrostatic properties of the membrane are hence insufficient to account for the variations in rhodopsin activation observed between POPC, DOPC, DOPE, and RDM lipids. Instead, we turn to a mesoscopic, mechanical explanation of these observations based on the individual lipid geometries unique to each membrane system (e.g., headgroup size and unsaturation).

DISCUSSION

Is a new biomembrane model necessary because of strong proteolipid coupling?

Our results are consistent with a picture in which cellular membrane function is influenced by mechanical properties of the membrane lipid bilayer (3–8,63–67). They point to strong in- and out-of-plane coupling interactions governing the activation of rhodopsin, which supersede the previous interpretation in terms of the fluid mosaic model (FMM). Notably, the FMM does not consider this strong proteolipid coupling, but rather the in-plane fluidity that affects rotational and translational diffusion of membrane proteins such as rhodopsin (21–24). One should nonetheless keep in mind that membranes are complex fluids, and are known to have a polymorphism that entails additional components of the stress tensor corresponding to shape transitions formulated in terms of principal curvatures (1,5). The present discoveries thus illuminate the insufficiency of the classical FMM, which allows only weak in-plane proteolipid coupling (20). In contrast to the FMM, we do not consider planar couplings in isolation that govern the gel to liquid-crystalline transition. Rather, we include the out-of-plane interactions giving rise to monolayer curvature associated with lamellar to nonlamellar phase transitions of the lipids.

In the case of rhodopsin, the evidence in favor of this view is the following. First, the shifting of the pH titration curve describing MII formation through protonation of Glu^{134} indicates a reversible modulation of the metarhodopsin equilibrium by membrane lipids. The bilayer lipid environment shifts the pK_A of Glu^{134} by over two pH units, meaning a lower pH is required to reversibly shift the metarhodopsin equilibrium to MII in the absence of native nonlamellar-forming lipids (25). Second, the modulation of the metarhodopsin equilibrium in response to a variety of lipid substitutions indicates a lack of chemical specificity to lipid type. Small lipid headgroups can be substituted for unsaturated acyl chains and vice versa (1,5). We hence eliminate the possibility of specific proteolipid interactions, such as those in lipid rafts (16,66), as the dominant governing factor. Both alterations to lipid headgroup (i.e., PE versus PC) and degree of unsaturation (i.e., 1-palmitoyl-2-oleoyl-*sn*-glycero- versus 1,2-dioleoyl-*sn*-glycerophospholipids) have similar effects on the metarhodopsin equilibrium, with the combined influences of both of these together having the greatest impact on rhodopsin energetics and strongly indicating the involvement of spontaneous curvature (1,5).

We next consider the implications of our results for the hydrophobic matching framework, wherein stretching or compression of the lipid chains increases the membrane potential energy to drive protein conformational changes (32). Here, the proteolipid coupling is strong and is only directed out of the plane. Because membrane expansion or compression requires an input of energy that can be modeled by Hooke's law, varying the equilibrium length of the lipid chains will affect the stability of expanded or contracted protein conformations. Yet, although hydrophobic matching can account for effects of acyl chain length (e.g., number of carbons) on rhodopsin activation (68), it predicts no effects of spontaneous monolayer lipid curvature on rhodopsin activation, a property arising from the combined effects of both lipid unsaturation and headgroup bulkiness on lipid-protein interactions (25). As an alternate explanation, we consider the lamellar versus nonlamellar polymorphisms for lipid bilayers (63,69,70). Among the canonical nonlamellar forms of lipids is the inverted hexagonal (H_{II}) phase, favored by unsaturated and small-headgroup lipids, in which pure DOPE can be found under standard biochemical conditions (69). The tendency of the membrane to adopt a nonlamellar polymorphism may couple to conformational changes within membrane proteins and is consistent with the results herein (5,31). Both increasing lipid unsaturation and decreasing lipid headgroup size, which lower the free energy inherent to the H_{II} phase, independently drive the conformational change of rhodopsin to the MII active state for the same reason—a tendency of the membrane to adopt a negative spontaneous monolayer curvature.

Flexible surface model for membrane lipid-protein interactions

In light of these observations, we next consider how our data align with the flexible surface model (1,5,25) of lipid-protein interactions (Fig. 1 *A*). The FSM predicts that conformational changes involved in rhodopsin activation should be governed by the elastic energy of curvature of the lipid membrane (31), as described for a neutral plane using differential geometry (5). Lipid composition gives rise to a spontaneous (intrinsic) curvature of the membrane describing the free-energy minimum. In turn, bending of the membrane to adopt the spontaneous curvature couples to protein conformational changes (1,2,4,51) and biochemical catalytic events (9,17,63) at the membrane level. Formulated in terms of the bending of a neutral plane with constant area per lipid, the FSM takes into account the lateral forces between lipids in addition to longitudinal (vertical) stresses. The FSM thus considers a Hookean, elastic behavior in two directions (both in plane and out of plane), as opposed to the mattress-model assumption of purely out-of-plane Hookean behavior (Fig. 1*B*). The FSM can account for the same phenomena, such as lipid length effects, detailed in the hydrophobic matching framework through the inclusion of a proteolipid solvation term that balances the elastic energy term contained in the monolayer curvature (5,31).

The current experimental findings show that greater lipid saturation and size of the phospholipid headgroups back shifts the rhodopsin equilibrium to the inactive MI state (Fig. 5). According to the FSM, both lipid saturation and headgroup size modulate the free energy of MII formation by changing the intrinsic, or spontaneous, curvature (H_0) of the membrane due to imbalances in the lateral pressure profiles of the lipids (31,71,72). Highly unsaturated lipids experience stronger lateral repulsive forces between the acyl chains, leading to an intrinsic negative curvature of a monolayer leaflet toward water. In a similar vein, decreasing the size of the phospholipid headgroup also produces a lateral pressure imbalance, in which the headgroup repulsions are smaller in magnitude than the acyl chain repulsions. Hence, both unsaturated acyl chains and small phospholipid headgroups contribute to a tendency of the membrane to adopt a negative monolayer curvature deformation ($H < 0$) toward water.

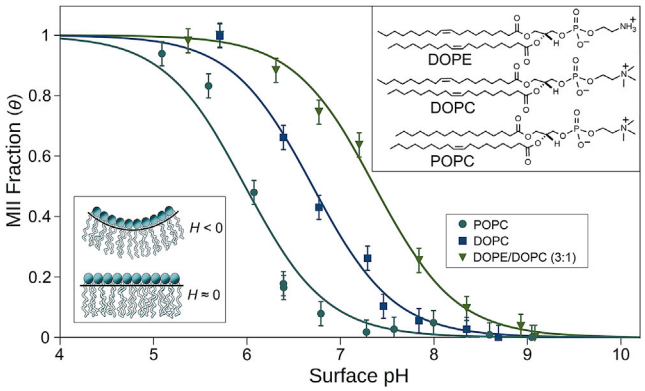

FIGURE 5 Rhodopsin activation in various membrane environments can be understood by frustration of the elastic curvature free energy. The metarhodopsin II fraction (θ) with protonated Schiff base is plotted versus surface pH at 10°C. Error bars correspond to uncertainties in the MII fraction propagated from the estimated errors in the spectral measurements ($\pm$ 4%). Note that the rhodopsin activation equilibrium undergoes a pK_A shift depending on both the lipid headgroups and acyl chains. Decreasing headgroup size (PE versus PC) or increasing acyl chain unsaturation (oleoyl versus palmitoyl groups) increases the active metarhodopsin II population. To see this figure in color, go online.

Combined influences of lipid acyl chains and polar headgroups reveal a fundamental connection to lipid polymorphism

As a general principle, we find that neutral DOPE lipids, which are both highly unsaturated and possess smaller phosphoethanolamine headgroups, provide a more conducive environment to rhodopsin activation than the larger-headgroup methylated DOPC and POPC lipids (51,73). In terms of the FSM, it therefore follows that the formation of active-state MII is facilitated by a negative membrane curvature of deformation. Altering the lipid composition to increase lateral pressure between the lipid acyl chains and decrease lateral pressure between headgroups will lower the free energy of membrane deformation, driving the metarhodopsin activation equilibrium forward. By contrast, increasing lipid saturation and headgroup size decreases absolute membrane intrinsic curvature, such that the free-energy cost of MII formation is high. We can use these trends to predict and assess the mechanisms of diverse lipid types on rhodopsin activation (25), with future work aimed at a deeper understanding of how electrostatic contributions to curvature balance other known surface charge effects (54,74).

At the protein level, the reason for the coupling between rhodopsin activation and negative bilayer curvature can be attributed to an overall expansion of rhodopsin during formation of the MII state, mediated by an outward movement of helix H6 by 5 Å and an extension of helix H5 compared with the dark state (75,76). This volumetric expansion has been experimentally shown by the effects of hydrostatic pressure (77,78), and osmotic pressure (37,79), as well as neutron scattering studies (80,81). It follows that a combination of mesoscopic-scale bilayer deformation properties in addition to specific lipid interactions modulates rhodopsin activation (63–67,82,83). In contrast to the standard biochemical view of GPCR activation governed completely by agonists and antagonists, we show how mechanical properties of the membrane (84) play equally important roles in rhodopsin modulation. We expect that the results acquired herein for the

FSM will have applicability in describing the protein-lipid interactions of other GPCRs and potentially other membrane proteins and peptides, as well (65).

CONCLUSIONS

The flexible surface model that we describe here supersedes the fluid mosaic model as a more accurate and inclusive paradigm of lipid-protein interactions (1,5). The FSM is a useful framework that is well poised to address a number of key unanswered questions in membrane biochemistry. On the side of expanding biophysical theory, we may use the stress field formulation of the FSM to consider the significance and causes of spatial organization at the membrane, including the interplay between membrane asymmetry and curvature-mediated lipid-protein interactions (85). Membrane protein oligomerization may be affected (68), as well as the formation of lipid microdomains and membrane fusion as it occurs in endo- and exocytosis and budding of enveloped viruses including HIV or coronavirus (10,11). Moreover, by formulating mechanisms of membrane-bound receptors and enzymes, as well as bilayer deformation involved in cytokinesis, phagocytosis, and viral budding in terms of the membrane stress field, we anticipate a breadth of physiological processes to be understood and engineered in terms of these concepts. How membrane curvature can be harnessed for biotechnological or biomedical applications represents a significant question for future research.

SUPPORTING MATERIAL

Supporting Material can be found online at https://doi.org/10.1016/j.bpj.2020.11.007.

AUTHOR CONTRIBUTIONS

M.F.B. and D.S.K. developed the initial concept. J.W.L., I.S., K.M.-M., M.M., and R.V. performed the major experiments. S.D.E.F. and J.W.L. carried out the analysis. S.D.E.F. and M.F.B. wrote the manuscript with discussion, review, and contributions from all authors.

ACKNOWLEDGMENTS

We thank B. Mertz for assistance with initial experiments and S. Bhagavatula for help with preparing figures.

This research was supported by the U.S. National Science Foundation (CHE 1904125 and MCB 1817862 to M.F.B.) and the U.S. National Institutes of Health (EY012049 and EY026041 to M.F.B. and EY029343 to D.S.K.). S.D.E.F. was partially supported by a Goldwater research scholarship.

REFERENCES

1. Brown, M. F. 1994. Modulation of rhodopsin function by properties of the membrane bilayer. *Chem. Phys. Lipids.* 73:159–180.
2. Brown, M. F. 1997. Influence of non-lamellar forming lipids on rhodopsin. *Curr. Top. Membr.* 44:285–356.
3. Phillips, R., T. Ursell, …, P. Sens. 2009. Emerging roles for lipids in shaping membrane-protein function. *Nature.* 459:379–385.
4. Soubias, O., and K. Gawrisch. 2012. The role of the lipid matrix for structure and function of the GPCR rhodopsin. *Biochim. Biophys. Acta.* 1818:234–240.
5. Brown, M. F. 2017. Soft matter in lipid-protein interactions. *Annu. Rev. Biophys.* 46:379–410.
6. Bassereau, P., R. Jin, …, T. R. Weikl. 2018. The 2018 biomembrane curvature and remodeling roadmap. *J. Phys. D.* 51:343001.
7. Corradi, V., B. I. Sejdiu, …, D. P. Tieleman. 2019. Emerging diversity in lipid–protein interactions. *Chem. Rev.* 119:5775–5848.
8. Lorent, J. H., K. R. Levental, …, I. Levental. 2020. Plasma membranes are asymmetric in lipid unsaturation, packing and protein shape. *Nat. Chem. Biol.* 16:644–652.
9. Schmick, M., and P. I. H. Bastiaens. 2014. The interdependence of membrane shape and cellular signal processing. *Cell.* 156:1132–1138.
10. Liang, R., J. M. J. Swanson, …, G. A. Voth. 2016. Acid activation mechanism of the influenza A M2 proton channel. *Proc. Natl. Acad. Sci. USA.* 113:E6955–E6964.
11. Paulino, J., X. Pang, …, T. A. Cross. 2019. Influenza A M2 channel clustering at high protein/lipid ratios: viral budding implications. *Biophys. J.* 116:1075–1084.
12. Hilgemann, D. W. 2003. Getting ready for the decade of the lipids. *Annu. Rev. Physiol.* 65:697–700.
13. Hilgemann, D. W., G. Dai, …, M. Fine. 2018. Lipid signaling to membrane proteins: from second messengers to membrane domains and adapter-free endocytosis. *J. Gen. Physiol.* 150:211–224.
14. Levental, I., and S. L. Veatch. 2016. The continuing mystery of lipid rafts. *J. Mol. Biol.* 428:4749–4764.
15. Rayermann, S. P., G. E. Rayermann, …, S. L. Keller. 2017. Hallmarks of reversible separation of living, unperturbed cell membranes into two liquid phases. *Biophys. J.* 113:2425–2432.
16. Engelman, D. M. 2005. Membranes are more mosaic than fluid. *Nature.* 438:578–580.
17. Lindblom, G., I. Brentel, …, Å. Wieslander. 1986. Phase equilibria of membrane lipids from *Acholeplasma laidlawii*: importance of a single lipid forming nonlamellar phases. *Biochemistry.* 25:7502–7510.
18. Morein, S., A.-S. Andersson, …, G. Lindblom. 1996. Wild-type *Escherichia coli* cells regulate the membrane lipid composition in a "window" between gel and non-lamellar structures. *J. Biol. Chem.* 271:6801–6809.
19. Wiedmann, T. S., R. D. Pates, …, M. F. Brown. 1988. Lipid-protein interactions mediate the photochemical function of rhodopsin. *Biochemistry.* 27:6469–6474.
20. Singer, S. J., and G. L. Nicolson. 1972. The fluid mosaic model of the structure of cell membranes. *Science.* 175:720–731.
21. Cone, R. A. 1972. Rotational diffusion of rhodopsin in the visual receptor membrane. *Nat. New Biol.* 236:39–43.
22. Liebman, P. A., W. S. Jagger, …, F. G. Bargoot. 1974. Membrane structure changes in rod outer segments associated with rhodopsin bleaching. *Nature.* 251:31–36.
23. Liebman, P. A., and G. Entine. 1974. Lateral diffusion of visual pigment in photorecptor disk membranes. *Science.* 185:457–459.
24. Poo, M.-m., and R. A. Cone. 1974. Lateral diffusion of rhodopsin in the photoreceptor membrane. *Nature.* 247:438–441.
25. Gibson, N. J., and M. F. Brown. 1993. Lipid headgroup and acyl chain composition modulate the MI–MII equilibrium of rhodopsin in recombinant membranes. *Biochemistry.* 32:2438–2454.
26. Mitchell, D. C., M. Straume, …, B. J. Litman. 1990. Modulation of metarhodopsin formation by cholesterol-induced ordering of bilayer lipids. *Biochemistry.* 29:9143–9149.

27. Litman, B. J., and D. C. Mitchell. 1996. A role for phospholipid polyunsaturation in modulating membrane protein function. *Lipids.* 31 (*Suppl*):S193–S197.

28. Thurmond, R. L., G. Lindblom, and M. F. Brown. 1993. Curvature, order, and dynamics of lipid hexagonal phases studied by deuterium NMR spectroscopy. *Biochemistry.* 32:5394–5410.

29. Brown, M. F. 1996. Membrane structure and dynamics studied with NMR spectroscopy. *In* Biological Membranes: A Molecular Perspective from Computation and Experiment. K. Merz, Jr. and B. Roux, eds. Birkhäuser, pp. 175–252.

30. Killian, J. A. 1998. Hydrophobic mismatch between proteins and lipids in membranes. *Biochim. Biophys. Acta.* 1376:401–416.

31. Brown, M. F. 2012. Curvature forces in membrane lipid-protein interactions. *Biochemistry.* 51:9782–9795.

32. Mouritsen, O. G., and M. Bloom. 1984. Mattress model of lipid-protein interactions in membranes. *Biophys. J.* 46:141–153.

33. Latorraca, N. R., A. J. Venkatakrishnan, and R. O. Dror. 2017. GPCR dynamics: structures in motion. *Chem. Rev.* 117:139–155.

34. Santos, R., O. Ursu, …, J. P. Overington. 2017. A comprehensive map of molecular drug targets. *Nat. Rev. Drug Discov.* 16:19–34.

35. Helfrich, W. 1973. Elastic properties of lipid bilayers: theory and possible experiments. *Z. Naturforsch. C.* 28:693–703.

36. Brown, M. F. 2012. UV-visible and infrared methods for investigating lipid-rhodopsin membrane interactions. *In* Membrane Protein Structure and Dynamics: Methods and Protocols. N. Vaidehi and J. Klein-Seetharaman, eds. Humana Press, pp. 127–153.

37. Chawla, U., S. M. D. C. Perera, …, M. F. Brown. 2020. Activation of the G-protein-coupled receptor rhodopsin by water. *Angew. Chem. Int. Ed. Engl*, Published online June 28, 2020.

38. Lewis, J. W., and D. S. Kliger. 2000. Absorption spectroscopy in studies of visual pigments: spectral and kinetic characterization of intermediates. *Methods Enzymol.* 315:164–178.

39. Thorgeirsson, T. E., J. W. Lewis, …, D. S. Kliger. 1993. Effects of temperature on rhodopsin photointermediates from lumirhodopsin to metarhodopsin II. *Biochemistry.* 32:13861–13872.

40. Jäger, S., I. Szundi, …, D. S. Kliger. 1998. Effects of pH on rhodopsin photointermediates from lumirhodopsin to metarhodopsin II. *Biochemistry.* 37:6998–7005.

41. Szundi, I., T. L. Mah, …, D. S. Kliger. 1998. Proton transfer reactions linked to rhodopsin activation. *Biochemistry.* 37:14237–14244.

42. Szundi, I., C. Funatogawa, and D. S. Kliger. 2016. Complexity of bovine rhodopsin activation revealed at low temperature and alkaline pH. *Biochemistry.* 55:5095–5105.

43. Szundi, I., C. Funatogawa, …, D. S. Kliger. 2017. Protein sequence and membrane lipid roles in the activation kinetics of bovine and human rhodopsins. *Biophys. J.* 113:1934–1944.

44. Bartl, F. J., and R. Vogel. 2007. Structural and functional properties of metarhodopsin III: recent spectroscopic studies on deactivation pathways of rhodopsin. *Phys. Chem. Chem. Phys.* 9:1648–1658.

45. Gruner, S. M., M. W. Tate, …, P. R. Cullis. 1988. X-ray diffraction study of the polymorphic behavior of N-methylated dioleoylphosphatidylethanolamine. *Biochemistry.* 27:2853–2866.

46. Gruner, S. M. 1989. Stability of lyotropic phases with curved interfaces. *J. Phys. Chem.* 93:7562–7570.

47. Shyamsunder, E., S. M. Gruner, …, C. P. S. Tilcock. 1988. Observation of inverted cubic phase in hydrated dioleoylphosphatidylethanolamine membranes. *Biochemistry.* 27:2332–2336.

48. Mahalingam, M., K. Martínez-Mayorga, …, R. Vogel. 2008. Two protonation switches control rhodopsin activation in membranes. *Proc. Natl. Acad. Sci. USA.* 105:17795–17800.

49. Sato, K., T. Yamashita, and Y. Shichida. 2014. Contribution of glutamic acid in the conserved E/DRY triad to the functional properties of rhodopsin. *Biochemistry.* 53:4420–4425.

50. Gibson, S. K., J. H. Parkes, and P. A. Liebman. 1999. Phosphorylation alters the pH-dependent active state equilibrium of rhodopsin by modulating the membrane surface potential. *Biochemistry.* 38:11103–11114.

51. Botelho, A. V., N. J. Gibson, …, M. F. Brown. 2002. Conformational energetics of rhodopsin modulated by nonlamellar-forming lipids. *Biochemistry.* 41:6354–6368.

52. Rand, R. P., N. L. Fuller, …, V. A. Parsegian. 1990. Membrane curvature, lipid segregation, and structural transitions for phospholipids under dual-solvent stress. *Biochemistry.* 29:76–87.

53. Kollmitzer, B., P. Heftberger, …, G. Pabst. 2013. Monolayer spontaneous curvature of raft-forming membrane lipids. *Soft Matter.* 9:10877–10884.

54. Tsui, F. C., S. A. Sundberg, and W. L. Hubbell. 1990. Distribution of charge on photoreceptor disc membranes and implications for charged lipid asymmetry. *Biophys. J.* 57:85–97.

55. Marsh, D. 2008. Energetics of hydrophobic matching in lipid-protein interactions. *Biophys. J.* 94:3996–4013.

56. Kinnun, J. J., K. J. Mallikarjunaiah, …, M. F. Brown. 2015. Elastic deformation and area per lipid of membranes: atomistic view from solid-state deuterium NMR spectroscopy. *Biochim. Biophys. Acta.* 1848:246–259.

57. Jensen, M. Ø., and O. G. Mouritsen. 2004. Lipids do influence protein function—the hydrophobic matching hypothesis revisited. *Biochim. Biophys. Acta.* 1666:205–226.

58. Tsui, F. C., D. M. Ojcius, and W. L. Hubbell. 1986. The intrinsic pK_a values for phosphatidylserine and phosphatidylethanolamine in phosphatidylcholine host bilayers. *Biophys. J.* 49:459–468.

59. Parkes, J. H., and P. A. Liebman. 1984. Temperature and pH dependence of the metarhodopsin I–metarhodopsin II kinetics and equilibria in bovine rod disk membrane suspensions. *Biochemistry.* 23:5054–5061.

60. Hubbell, W. L. 1990. Transbilayer coupling mechanism for the formation of lipid asymmetry in biological membranes. Application to the photoreceptor disc membrane. *Biophys. J.* 57:99–108.

61. Wang, Y., A. V. Botelho, …, M. F. Brown. 2002. Electrostatic properties of membrane lipids coupled to metarhodopsin II formation in visual transduction. *J. Am. Chem. Soc.* 124:7690–7701.

62. Delange, F., M. Merkx, …, W. J. DeGrip. 1997. Modulation of the metarhodopsin I/metarhodopsin II equilibrium of bovine rhodopsin by ionic strength. Evidence for a surface-charge effect. *Eur. J. Biochem.* 243:174–180.

63. Lindblom, G., and L. Rilfors. 1989. Cubic phases and isotropic structures formed by membrane lipids – possible biological relevance. *Biochim. Biophys. Acta.* 988:221–256.

64. Lee, A. G. 2004. How lipids affect the activities of integral membrane proteins. *Biochim. Biophys. Acta.* 1666:62–87.

65. Andersen, O. S., and R. E. Koeppe, II. 2007. Bilayer thickness and membrane protein function: an energetic perspective. *Annu. Rev. Biophys. Biomol. Struct.* 36:107–130.

66. van Meer, G., D. R. Voelker, and G. W. Feigenson. 2008. Membrane lipids: where they are and how they behave. *Nat. Rev. Mol. Cell Biol.* 9:112–124.

67. Honerkamp-Smith, A. R., S. L. Veatch, and S. L. Keller. 2009. An introduction to critical points for biophysicists; observations of compositional heterogeneity in lipid membranes. *Biochim. Biophys. Acta.* 1788:53–63.

68. Botelho, A. V., T. Huber, …, M. F. Brown. 2006. Curvature and hydrophobic forces drive oligomerization and modulate activity of rhodopsin in membranes. *Biophys. J.* 91:4464–4477.

69. Seddon, J. M. 1990. Structure of the inverted hexagonal (H_{II}) phase, and non-lamellar phase transitions of lipids. *Biochim. Biophys. Acta.* 1031:1–69.

70. Marsh, D. 2013. Handbook of Lipid Bilayers. CRC Press/Taylor & Francis Group, Boca Raton, FL.

71. Cantor, R. S. 1999. The influence of membrane lateral pressures on simple geometric models of protein conformational equilibria. *Chem. Phys. Lipids.* 101:45–56.

72. Marsh, D. 2008. Protein modulation of lipids, and vice-versa, in membranes. *Biochim. Biophys. Acta.* 1778:1545–1575.

73. Soubias, O., W. E. Teague, Jr., …, K. Gawrisch. 2010. Contribution of membrane elastic energy to rhodopsin function. *Biophys. J.* 99:817–824.

74. Gibson, N. J., and M. F. Brown. 1991. Membrane lipid influences on the energetics of the metarhodopsin I and metarhodopsin II conformational states of rhodopsin probed by flash photolysis. *Photochem. Photobiol.* 54:985–992.

75. Altenbach, C., A. K. Kusnetzow, …, W. L. Hubbell. 2008. High-resolution distance mapping in rhodopsin reveals the pattern of helix movement due to activation. *Proc. Natl. Acad. Sci. USA.* 105:7439–7444.

76. Choe, H. W., Y. J. Kim, …, O. P. Ernst. 2011. Crystal structure of metarhodopsin II. *Nature.* 471:651–655.

77. Lamola, A. A., T. Yamane, and A. Zipp. 1974. Effects of detergents and high pressures upon the metarhodopsin I–metarhodopsin II equilibrium. *Biochemistry.* 13:738–745.

78. Attwood, P. V., and H. Gutfreund. 1980. The application of pressure relaxation to the study of the equilibrium between metarhodopsin I and II from bovine retinas. *FEBS Lett.* 119:323–326.

79. Fried, S. D. E., A. R. Eitel, …, M. F. Brown. 2020. G-protein-coupled receptors are solvent-swollen in the functionally active state. *Biophys. J.* 118:527A.

80. Shrestha, U. R., S. M. D. C. Perera, …, X.-Q. Chu. 2016. Quasi-elastic neutron scattering reveals ligand-induced protein dynamics of a G-protein-coupled receptor. *J. Phys. Chem. Lett.* 7:4130–4136.

81. Perera, S. M. D. C., U. Chawla, …, M. F. Brown. 2018. Small-angle neutron scattering reveals energy landscape for rhodopsin photoactivation. *J. Phys. Chem. Lett.* 9:7064–7071.

82. Bloom, M., E. Evans, and O. G. Mouritsen. 1991. Physical properties of the fluid lipid-bilayer component of cell membranes: a perspective. *Q. Rev. Biophys.* 24:293–397.

83. Salas-Estrada, L. A., N. Leioatts, …, A. Grossfield. 2018. Lipids alter rhodopsin function via ligand-like and solvent-like interactions. *Biophys. J.* 114:355–367.

84. Khelashvili, G., P. B. C. Albornoz, …, H. Weinstein. 2012. Why GPCRs behave differently in cubic and lamellar lipidic mesophases. *J. Am. Chem. Soc.* 134:15858–15868.

85. Eicher, B., D. Marquardt, …, G. Pabst. 2018. Intrinsic curvature-mediated transbilayer coupling in asymmetric lipid vesicles. *Biophys. J.* 114:146–157.